Annular Condensation CFD Models for the Water-Steam in the Heat Pipe Systems

H. El Mghari[1], R. El Amraoui[1,*], H. Grimech [2], Z. Ihsane[2] , M. Mouqallid[3]

1 LAMET laboratory, Faculty of Science and Technics, Sultan Moulay Slimane Univ., Béni Mellal, Morocco
2 Laboratory of Materials Physics, Faculty of Science and Technics, Sultan Moulay Slimane Univ., Béni Mellal, Morocco.
3 Dep. of energy, ENSAM, Moulay Ismail Univercity, Morocco.

Abstract

This paper describes a CFD based strategy for the modelling of two-phase flows condensation in LHP system's with heat and mass transfer using ANSYS FLUENT 13. Multiphase Volume of Fluid (VOF) model is used to track the interface and standard k-ϵ model was adopted for modelling the turbulence. Effects of wall temperature and vapour injection velocity are explored to understand the hydrodynamic and thermal characteristics of the capillary condensation process. In addition, the effect of both these parameters on the rate of condensation is investigated. The technique is based on a recently derived phase field model for boiling and condensation phenomena. The results showed that the phase field model fit best the literature's results.

Nomenclature

CFD   computational fluid dynamics
CSF   continuous surface force
E   energy per unit mass (J/kg)
f   friction factor (-)
F   force (N)
G   mass flux (kg/m²s)
h   heat transfer coefficient (W/m²)
hlv   latent heat (J/kg)
k   thermal cpnductivity (W/m K)
L   Annular condensation length (m)
MAE   mean absolute error (%)
m   Mass flux (kg s-1)
P   pressure (Pa)
q   heat flux (W/m²)
r   relaxation factor (-)
Sh   energy source term (kg/m s3)
t   time (s)
T   temperature (K)
v   velocity (m/s)
VOF   Volume of Fluid
x   abscissa (m)

Greek symbols

ε   void fraction (-)
λ   thermal conductivity (W/mK)
μ   Viscosity ($kg\,m^{-1}\,s^{-1}$)
ρ   Density ($kg\,m^{-3}$)
σ   Surface tension (N m-1)

Subscripts

av   average
cell   cell
con   condenser
l   liquid
m   mean
v   vapor
s   saturation

1. Introduction

The capillary condensation is an important process in a various engineering fields, including space technology, defence systems, aerospace applications, manufacturing technology, industrial processes and consumer electronics. As shown in Fig. 1, conventional heat pipes have structures which consist of evaporation, adiabatic (transport) and condensation section. The heat is transferred to the evaporation zone by conduction through the pipe wall and wick structure, and vaporizes the working fluid. The vapor pressure then drives the vapor through the adiabatic zone to the condenser zone. At condenser, the vapor condenses and releases its latent heat of

vaporization to the heat sink. The capillary pressure created by the wick structure pumps the condensed fluid back to the evaporator. Thus, the heat pipe can continuously transport the latent heat of vaporization from the evaporator to the condenser.Microchannel condensation has the advantages of high heat transfer coefficients, large area-to-volume ratios and the potential of reducing the required working fluid charge. The high heat transfer rates for condensation in microchannels has been investigated in recent years with the focus on the two-phase flow patterns [1–3], the pressure drop [4] and the influence of the microchannel cross section [5-7]. Studies have shown that the condensation flow patterns in microchannels differ significantly from those in large channels [8] and millimetre size channels.
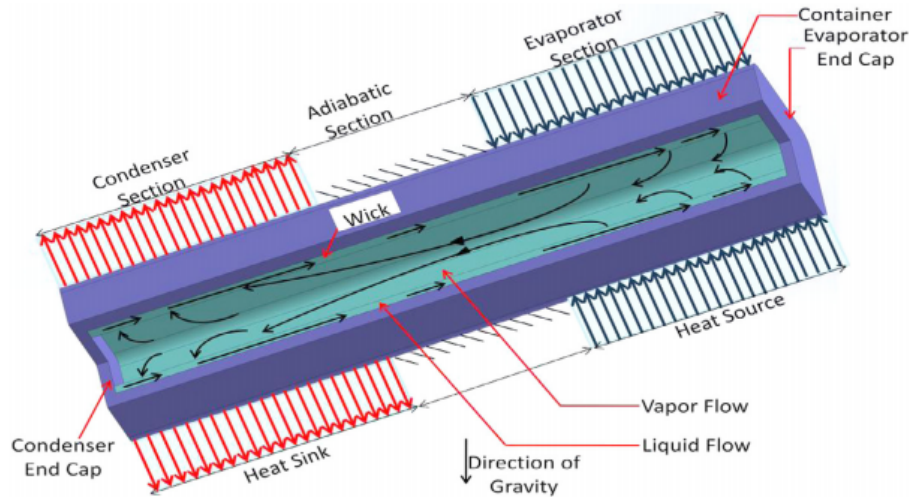
Figure 1: Schematic of a conventional heat pipe with principle of operation[9]

The development of CFD codes for simulation of the heat pipes and heat pipe exchangers is a relatively new field of research. It has been receiving renewed interest due to recent advances in computing which allow the simulation of the phase change within the heat pipe. However, the phase change models found in the literature can be grouped in five categories (Table 1). The first collects semi empirical correlations, among which the most used one is the surface renewal model[10-15], where the condensation rate is calculated from the liquid turbulent quantities. In this model, the condensation rate is controlled by renewal period of turbulent eddies traveling from the bulk supercooled liquid to the liquid vapor interface. The Very Large Eddy Simulations (VLES) and the surface divergence model to calculate the condensation rate are used. In the second group, expressions for condensation and evaporation rates are derived from the kinetic theory of gases [16]. These models require a good resolution of the interfacial region and, thus, their application at the scale of the VOF method is arguable. The third category is the numerical iteration technique introduced by Lee [17]. Liu et al.[18] also derived a similar expression for the condensation rate from the Hertz-Knudsen gas kinetic model in ANSYS Fluent 12 for the Euler-Euler two-phase model, but the implementation is equivalent to that of the numerical iteration technique.

In the fourth group are the models that make use of the heat flux balance (Stefan condition) at the liquid-vapor interface [19]. In this case, the condensation rate depends on the temperature gradient on both sides of the interface and, therefore, the application to models such as VOF—where only one temperature field exists for the two phases— is not straightforward. Sato and Niceno [20] calculated the interfacial mass transfer rate directly from the heat flux balance equation to simulate nucleate boiling, finding good agreement with experiments. Other authors [21,23] implemented the heat flux balance equation in FLUENT, considering equal temperature gradient and thermal conductivity on the gas and liquid side, however, they did not compare temperature fields to experiment, only the characteristics of the flow patterns were assessed. In the fifth group is the general phase field model developed by Badillo [24]. He applied the model for bubble growth under convective conditions, achieving good results compared to experiments for the bubble growth rate [25].

The present study proposes a purely CFD, transient model for condensation heat transfer process in the horizontal heat exchangers. The formulation is not restricted to a single bubble or a specific flow regime, but is targeted at the simulation of all condensation flow patterns, especially annular flow. The model has been implemented for a relatively simple geometry, a single microchannel, for which well-established experimental results are available in the literature. The predictions of two-phase pressure drop and heat transfer coefficient have been compared against the experimental visualization data. Additionally, condensation annular flow characteristics (temperature, void fraction, velocity…) have been simulated.

Table 1. Modeling strategies for phase change phenomena - literature review.

1. Semi-empiricalcorrelations			
(a) surface renewal			
CFX	two-fluid model	condensation	(Egorov [11] ; Scheuerer [14])
NEPTUNE_CFD	two-fluid model	condensation	(Egorov, [11] ; Štrubelj et al [15])
CFX	VOF	condensation	(Ceuca and Macián-Juan, [10])
(b) surface divergence			
TransAT	level set	condensation	(Lakehal and Labois, [12])
2. Kinetic theory of gases (Collier, [16])			
n.i.*	VOF	condensation	(Collier, [16])
OpenFOAM	VOF	boiling	(Kunkelmann and Stephan [13])
FLUENT	VOF	boiling	(Hardt and Wondra, [19])
3. Numericaliteration technique (Lee, [17])			
FLUENT	VOF	condensation	(Liu et al.[18])
4. Heat flux balance			
(a) Separate temperature gradient in the phases			
PSI-BOIL		boiling	(Sato and Niceno, [20])
n.i.	VOF	condensation	(Liu et al.[18])
OpenFOAM	VOF	boiling	(Hardt and Wondra, [19])
(b) Equal temperature gradient			
FLUENT	LS + VOF	boiling	(Nichita, [21])
FLUENT	VOF	boiling	(Ganapathy et al., [22])
(c) Gas thermal conductivity zero			
FLUENT	VOF	boiling	(Sun et al., [23])
5. Phase field model			
PSI-BOIL		boiling	(Badillo, [25])

2. Numerical simulation

2.1. Governing Equations

ANSYS Fluent is used to perform the numerical work. The volume of fluid (VOF) model is adopted to capture the liquid-vapour interface in this simulation. This model accomplishes interface tracking by solving an additional continuity-like equation for the volume fraction. The two phases are assumed to be incompressible and not penetrate each other. The sum of the volume fractions of the two phases in each cell is unity. Properties of a single fluid are calculated based on the volume weight fraction of each phase in the cell. In the present work, the mathematical model is composed by a set of conservation laws for mass, momentum and energy, this is (ANSYS, Inc., 2013) [26]:

$$\frac{\partial \rho}{\partial t} + \nabla(\rho \vec{v}) = 0 \tag{1}$$

$$\frac{\partial(\rho \mathbf{V})}{\partial t} + \nabla(\rho \vec{v}\vec{v}) = -\nabla P + \nabla[\mu(\nabla \vec{v} + \nabla \vec{v}')] + \vec{F} \tag{2}$$

$$\frac{\partial(\rho E)}{\partial t} + \nabla[\vec{v}(\rho E)] = \nabla(\lambda_e \nabla T) + S_h \tag{3}$$

where ρ is the density, P is the static pressure, T is the temperature, v is the velocity, μ is the molecular viscosity and F is the external body force, λ_e is the effective thermal conductivity, S are source terms and $E = h - P/\rho + v^2/2$ is the total energy per unit volume. Despite that the VOF method assumes that coexisting phases are not interpenetrating, an additional variable - the void fraction (ϵ) - is introduced to calculate the mixture properties of the fluid in the cells containing the interfacial region. By defining the mass of each phase in terms of the void fraction, we can express mass conservation for each phase as:

$$\frac{\partial \rho}{\partial t}(\epsilon_k \rho_k) + \nabla(\epsilon_k \rho_k \vec{v}_k) = S_{\epsilon k} \tag{4}$$

where volume conservation requires that $\sum_{k=1}^{n} \epsilon_k = 1$. For the mixture of vapor and liquid, the phases are defined as follows: n = 2, $k = v, l$, and the mixture properties are obtained by adding the contribution from each phase (e.g. $\rho = \rho_l \epsilon_l + \rho_v \epsilon_v$). The total energy of the mixture is defined as:

$$E = \frac{\sum_{k=1}^{n} \epsilon_k \rho_k E_k}{\sum_{q=1}^{n} \epsilon_k \rho_k} \tag{5}$$

where E_k for each phase is based on the specific heat of that phase and shared temperature. The source term, S_h is the volumetric heat source term. In order to simulate the heat transfer between the phases during the bubble condensation, modeling the heat source term is required.

2.2. Phase change modelling

The mass transfer between the phases introduce additional sources in the conservation equations. The heat source (S_h) related to the phase change, is calculated from the interfacial mass transfer rate per unit volume ($\dot{m} = S_{v\epsilon} = -S_{l\epsilon}$) multiplied by the latent heat (h_{lv}), that is

$$S_h = \dot{m}\, h_{lv} \quad (6)$$

where $\dot{m}$ is calculated from the three condensation models introduced below.

## 2.3. Numerical iteration technique

The numerical iteration technique [17] enforces a constant saturation temperature in the bulk vapor as well as at the liquid-vapor interface. Thus, if the temperature of an interfacial cell($i.e.\ 0 < \epsilon < 1$) differs from saturation, then the mass evaporation rate is calculated from the local superheating (or supercooling) as:

$$\dot{m}_v = \begin{cases} -r\rho_v\epsilon_v \frac{(T_{cell}-T_s)}{T_s}; & \text{if } T_{cell} < T_s \\ -r\rho_l\epsilon_l \frac{(T_{cell}-T_s)}{T_s}; & \text{if } T_{cell} > T_s \end{cases} \quad (7)$$

The relaxation factor r sets an arbitrary frequency scale ($i.e.\ time^{-1}$) at which the phase change takes place. Low values of the relaxation factor cause serious deviation from the saturation temperature in the interfacial cells, and high r values cause difficulties in the convergence of the solver. Therefore, the relaxation factor has to be tuned such that a compromise is found between the final result and the convergence speed.

2.4. Geometry and mesh

Geometry of a horizontal two-dimension wickless heat pipe has been generated using workbench design modular (Ansys13). The geometry represents a copper channel with a total height of 20 mm, outer and inner diameters of 0.5 mm respectively. The heat pipe is divided into three sections, evaporator (20 mm) condenser (20 mm) and adiabatic zone with height of 40 mm each as illustrated in Fig. 2. These dimensions are chosen to be similar to geometry of a previous experimental work by Abdullahi [27] to validate the CFD simulation.
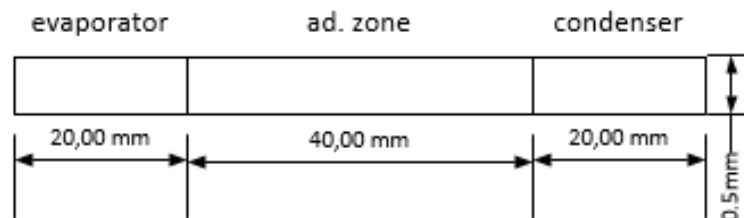

Figure 2: Heat pipe geometry

Workbench design modular (Ansys 13) was also used to mesh the geometry where Control edge sizing technique was employed to control the grid in every domain and to govern cell sizes nearinner walls and inside the solid domain (walls) with bias factor of 10 used in these regions to ensure that the flow and heat transfer can be correctly captured in these areas. The number of cells in the fluid domain was 24,113and 9350 grids in the solid domain. The mesh size and type are shown in Fig. 3.

The initial temperature of both condenser wall and liquid should be selected slightly above the boiling point which was chosen to be 373 K to insure that the boiling process occurs once simulation time starts to reduce computational time and the condenser wall and fluid temperatures were set as 290 K (condenser cooling temperature). Operating temperature should beset to be the smallest temperature in the system (290 K) and operating density must be set as 0 kg/m3 when ideal gas is used and as the smallest density in the system when constant gas density is used. In addition, saturation temperature and operating pressure were set to be 373 K and 101325 Pa, respectively.

At the internal walls of condenser sections, a non-slip boundary condition is applied, while a constant heat flux is imposed at the outer wall to simulate the heat added to the microchannels. Two values of mass flux were employed $119\ and\ 125 kg/m^2s$. The top and the bottom ends of the system is assumed to be insulated, which means no cooling or heating effect applied at these walls. As a result, a zero heat flux is defined at these ends.
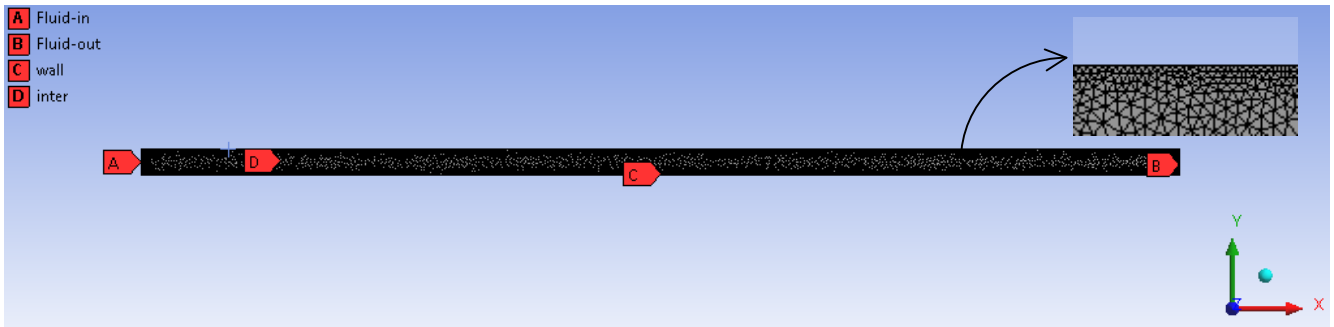
Figure 3 :Mesh of zoomed section.

To model the heat removed from the condenser section, a convection boundary condition is applied at the outer wall of the condenser section. Thus, the heat transfer coefficient between cooling water and the condenser's wall needs to be calculated from the following relation:

$$h = \frac{q_{con}}{\Im\, L_{con}(T_{c,av} - T_m)} \qquad (8)$$

where h is the convection heat transfer coefficient between thecooling water and the condenser's wall, q_{con} is the heat removed from the condenser section, $T_{c,av}$ is the average wall temperatureof the condenser section and T_m is the mean temperature of thecooling water. Values of q_{con}, and $T_m$are obtained from the experimental investigations [30]. To include the effect of the interfacial force between liquid and vapour, the term $\vec{F}$is added to the momentum equation Eq. (2) by activating the continuous surface force CSF in the fluent. Consequently, the value of the surface tension in Eq. (6) can be computed from the following formula [17]:

$$\sigma = 0.09805856 - 1.845 * 10^{-5}T - 2.3 * 10^{-7}T^2 \qquad (9)$$

2.5. Solution methods and techniques

In present analysis, the VOF model is used to simulate the multi-phase flow, while the gravitational acceleration is negligible (body force term) i.e. capillary regime. Water was used as the working fluid, whose thermophysical properties at the saturation temperature corresponding to an operating pressure 1bar were obtained from the material database of Fluent, are shown in table 2. The water liquid is chosen to be a secondary phase (liquid phase). A transient solution with a time step of 0.001 s is employed for all cases due to dynamic behavior of the two-phase flow [29, 30].A combination of the SIMPLE algorithm for pressure-velocity coupling and first-order upwind scheme for the calculation of the momentum and energy are used [31] and standard k-ϵ model was adopted for modeling the turbulence [32-33]. For determination of the volume fraction and pressure, Geo-Reconstruct and PRESTO discretization are chosen, respectively [28,29]. The solution is considered to be converged when the residuals of the mass and velocity components are reduced to 10^{-4} while the residuals of the temperature variables are reduced to 10^{-6}.

Table 2. Properties of working fluids used in the simulation

Properties	Water-liquid	water-vapor
Density(kg/m^3)	1000	0.5542
Cp($J/kg.K$)	4182	2014
Thermal conductivity (W/m.K)	0.6	0.0261
Viscosity (kg/m.s)	0.009	$1.34\ 10^{-5}$
Molecular Weight(kg/kgmol)	18.015	18.0152
Reference temperature (K)	298.15	298.15

3. Results and discussion

3.1. Condensation heat transfer and validation model

Annular flow is a stable condensation flow pattern widely occurred in the microchannel at high vapor velocity because condensate film is entrained from the microchannel under shear stress at the liquid – vapor interface. For annular flow, vapor has enough energy to move up the condensate film. In this study, the CFD model developed focus in the capillary annular condensation phenomena. The validation, verification and

+%25

implementation of the CFD studies are conducted using the geometry and experimental data from the available literature by El Mghari and Louahlia [30]. In their studies, the microchannel was employed to experimentally study the condensation process of water vapor flows. The local heat transfer coefficients estimated using the proposed model are compared to the measurements for steam condensation in the microchannel. Calculations are conducted for each inlet vapor mass flux using the measured heat fluxes as a boundary condition. Experimental heat fluxes are interpolated using an exponential form as

$$q_x = q_0 e^{-nx} \tag{10}$$

where q_0 and n are defined from the experimental results for each inlet mass flux and x is the dimensionless abscissa defined by Eq. (10). According to the same experimental conditions, we measured and numerically calculated the local condensation heat transfer coefficient for each inlet vapor mass velocity. The results of the computed local condensation heat transfer coefficient versus the measured values are presented in Fig. 4. showing that the local experimental results are close to those predicted by the CFD model. The small gap between the numerical results and measurements is due to the simplifying assumptions of the model on the one hand and uncertainty in the measurements at microscale channel. The comparison of these results is presented in Fig.5. It can be seen that the predicted local condensation heat transfer coefficients from the numerical model agree with experimental data with a maximum mean absolute error about ±25%.
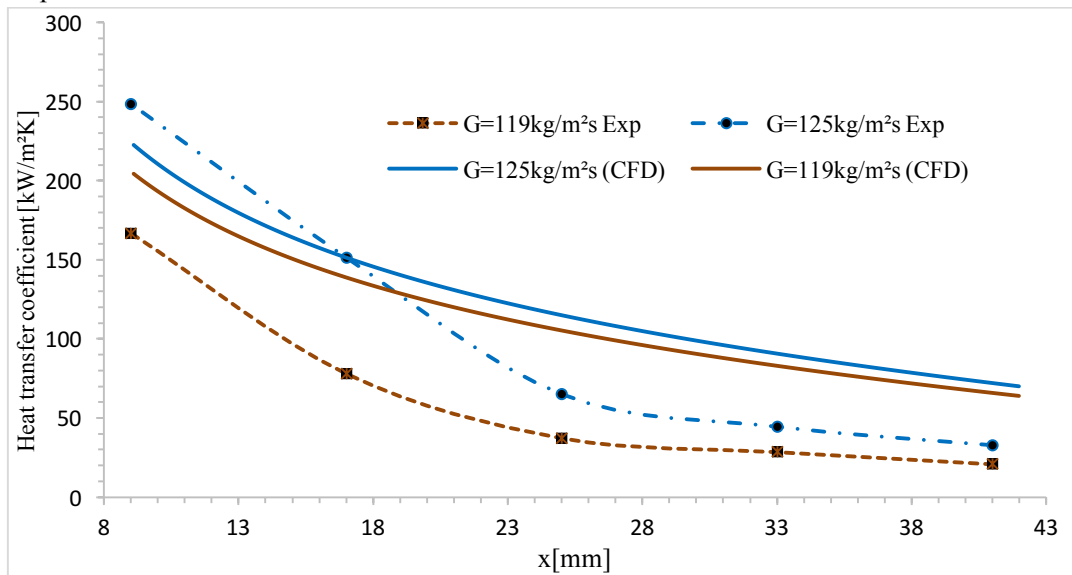

Figure 4: Direct comparison between the experimental and the predicted local condensation heat heat transfer rate
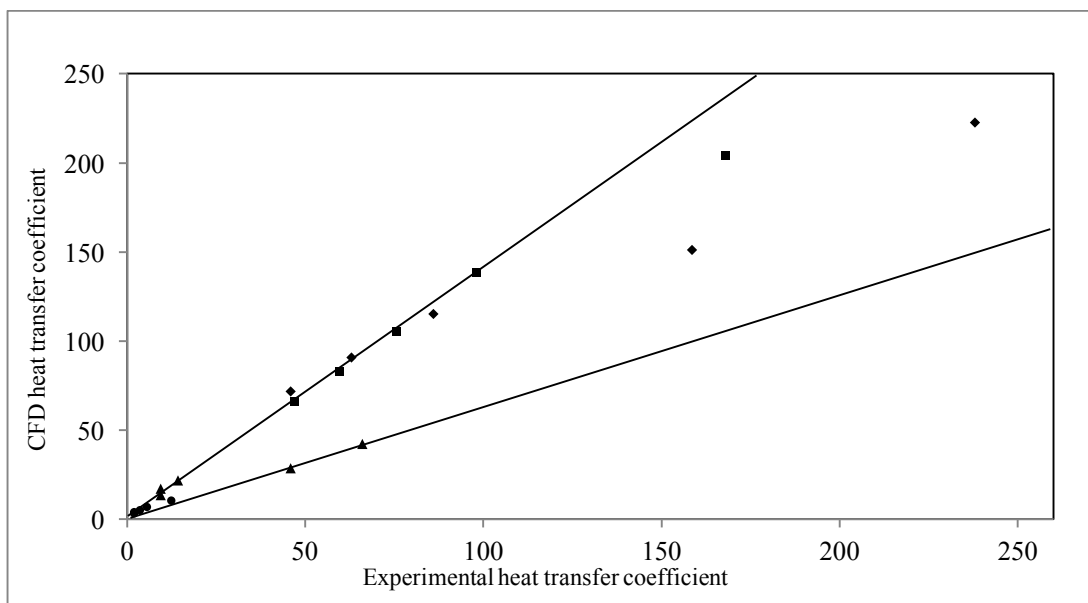

Figure 5: Comparison between experimental local heat transfer coefficient and the CFD model.

3.2. Void fraction

Fig. 6 depicts the vapor and the liquid void fraction distribution along the channel under conditions of almost the different inlet vapor Reynolds number with a constant external wall heat flux($q_0 = 7\ 10^5 w/m^2$). The vapor phase decreases along the channel, and it is lower under the lower inlet vapor mass flux. The explanation is that the small condensation length with lower inlet mass flux (i.e. lower inlet vapor Reynolds) results in a more latent heat. Hence, the vapor with high temperature is easier to directly contact with the cool channel wall, and thus the good performance of flow condensation heat transfer induces mild decrease in wall temperature before the injection flow. As mentioned above, with the lowing of inlet mass flux, the annular condensation becomes indistinct and the channel wall tends to be covered by condensate film, which weakens the flow condensation heat transfer performance.
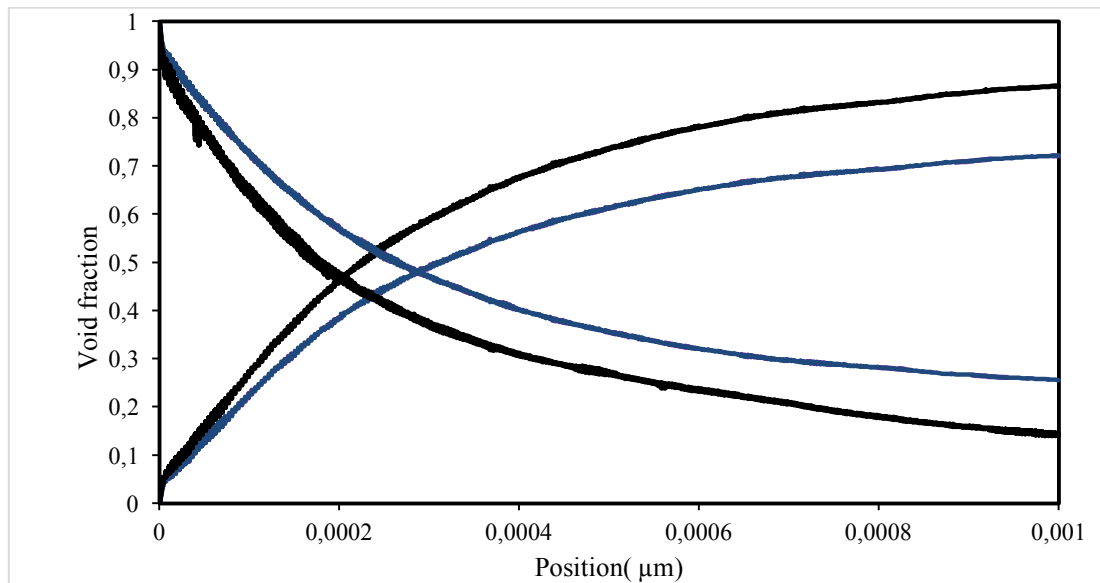

Figure 6: Void fraction versus abscissa position ($G = 119\ and\ 125 kg/m^2 s)\ q_0 = 7\ 10^5 w/m^2$)

Annular flow reported in Fig. 7 is typically characterized by a core of vapor flowing through the center of the channel surrounded by a thin film of liquid along the channel wall. Both have been compared against the visualization data of literature, and a good resemblance was obtained. While smooth annular flow comprises a relatively straight/flat interface profile, the wavy annular flow regime is characterized by a wavy interfacial profile comprising crests and troughs. It is noted that the liquid and vapor phases can move at different velocities, and when this is a dominant occurrence, the resulting shear forces at the interface lead to the formation of waves Fig.8.Some authors used an optical interference technique to obtain the topology of the interface and the above-described the instabilities were reported to have amplitude on the order of a few microns.
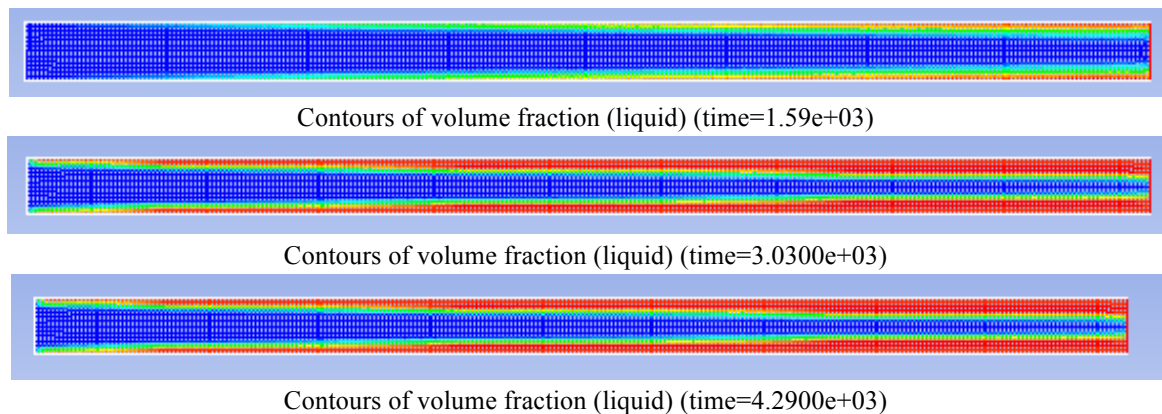

Contours of volume fraction (liquid) (time=1.59e+03)

Contours of volume fraction (liquid) (time=3.0300e+03)

Contours of volume fraction (liquid) (time=4.2900e+03)

Figure 7: Temporal evolution of the void fraction versus abscissa position (G=119kg/m²s)

3.3. Pressure, temperature and velocity repartitions

In this section, the condensation process of the water vapor is numerically calculated in the above mentioned heat pipe condenser at the inlet pressure of 151325Pa and temperature of 373.15 K. Fig. 8.a shows the computational contours of the temperature in the microchannel at the beginning annular condensation phenomena, and the detailed information of the pressure along the condenser section is described in Fig. 8.b. It can be observed that the mixture pressure decrease as the abscissa increase. This can be explained that the change of the latent heat between the phase transition processes from the vapor to liquid will heat the water vapor. Figs. 8.c and 8.d show the velocity repartition during the water vapor condensation process. We can see that the high velocity in the center line, and it rapidly drop to the minimum value of about zero m/s at the wall (friction forces effects).

(a)

(b)

-c-

-d-
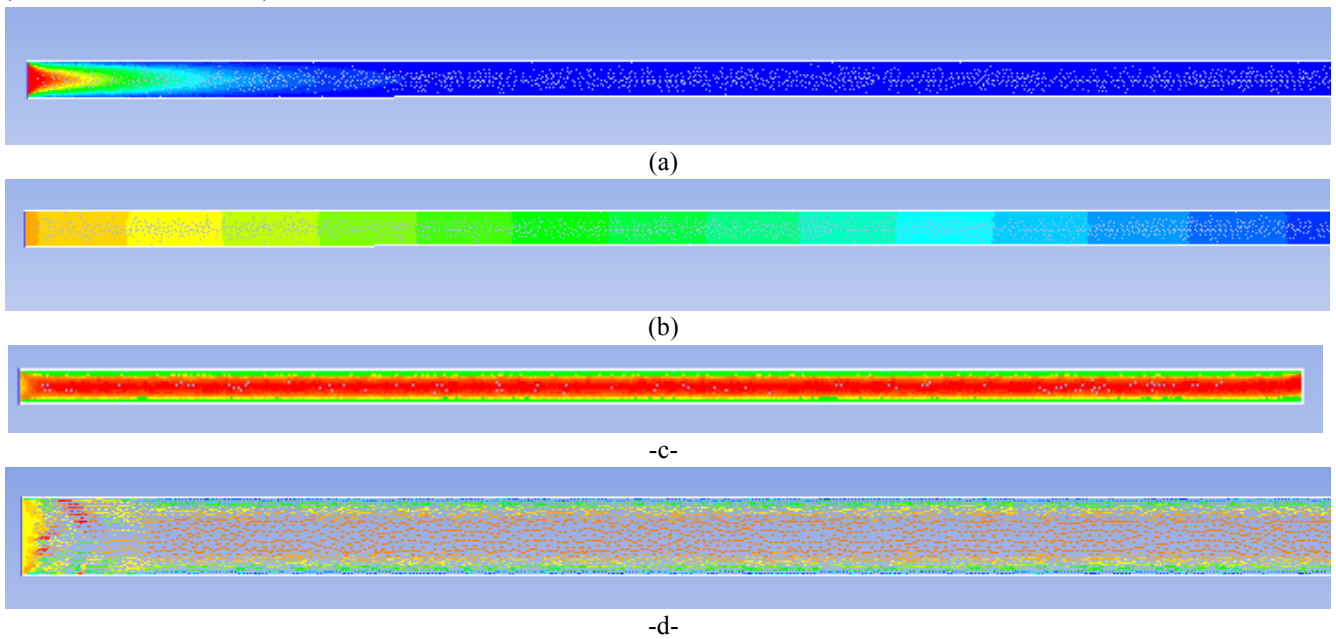
Figure 8: annular flow characteristics: - a: temperature, b: pressure, c: velocity and d: zoomed velocity (G=119kg/m²s)

Conclusion

A numerical (CFD) investigation was performed to investigate the flow condensation of water vapour in a wide range of inlet vapour Reynolds number inside a several forms of heat pipes. The condensation flow patterns of pure water vapour in the microchannel under different inlet vapour mass flux are presented and analyzed. In addition, the effect of external heat flux on condensation flow and the effect of some parameters on heat transfer performance are discussed. Finally, the main conclusions are drawn as follows:

- The local heat transfer coefficient increases with increasing vapour Reynolds number, and it decreases with increasing abscissa position along the condenser section.
- The higher inlet vapour Reynolds number and external heat flux greater than$(q_0 = 5 \ 10^5 w/m^2)$ are necessary conditions for condensation annular flow inside microchannel with *500 µm* of hydraulic diameter.
- The wall temperature decreases along the flow direction. Especially, under a lower inlet vapour mass flux. This is explained by the increase of the thermal resistance in the intern wall (increase of the thin film thicknesses)
- This study provided a detailed understanding of various aspects of heat pipe condensation. The user defined code will be used to analyze the thermal behaviour of the heat transfer system which heat pipes from.
- The maximum variation between the CFD computational results and experimental data was found to be 25%

References
1. X.J. Quan, P. Cheng, H.Y. Wu, *Int. J. Heat Mass Transf.* 51 (3–4) (2008) 707–716.
2. Ma X.H., Fan X.G., Lan Z., Hao T.T., J. *Micromech. Microeng.* 21(7) (2011) 075009.
3. Zhang W., Xu J., Thome J.R.,*Int. J. Heat Mass Transf.* 51 (13) (2008) 3420–3433.
4. X. Fan, X. Ma, L. Yang, Z.Lan, T. Hao, R. Jiang, T. Bai, *Exp. Therm. Fluid Sci.* 76 (2016) 45–56.

5. Hao T.T., Ma X.H., Lan Z., Jiang R., Fan X*., Int. J. Heat Mass Transf.* 66 (2013) 745–756.
6. Chen Y.P., Wu R., Shi M.H., Wu J., Peterson G.P., *Int. J. Heat Mass Transf.* 52 (21–22) (2009) 5122–5129.
7. El Mghari, H. ;Asbik, M., Louhlia, H*., Appl. Therm. Eng*64(2014) 358-370.
8. Xing F., Xu J., Xie J., Liu H., Wang Z., Ma X., *Int. J. Multiphase Flow* 71 (2015) 98–115.
9. Panda K.K. , Dulera I.V., Basak A., to appear in *Nuclear Engineering and Design* (2017)
10. Ceuca, S.C., Macián-Juan, R., ICONE-20. *Anaheim, California*, USA (2012) No. 54347.
11. Egorov, Y., *Technical Report Ansys, Germany*, EVOL-ECORA-D07 (2004)
12. Lakehal, D., Labois, *M.,. Int. J. Multiphase Flow* 37 (2011), 627–639.
13. Kunkelmann, C., Stephan, P., *Numer. Heat Transfer* 56(2009), 631–646.
14. Scheuerer, M., *Technical Report. GRS, Germany*, NURESIM-SP2-TH, (2006), D.2.1.4.1.
15. Štrubelj, L., Ézsöl, G., Tiselj, I., *Nuclear Eng. Des. 240* (2010)266–274.
16. Collier, J.G., *Clarendon Press, Oxford, UK.*, (1996) ISBN-978-0-19856-296-2.
17. Lee, W.H., *Multiphase Transp.* (1980), 407–432.
18. Liu, Z., Sunden, B., Yuan, J., *Heat Transfer Res.* 43 (2012) 47–68.
19. Hardt, S., Wondra, F., *J. Comput. Phys.* 227(2008), 5871–5895.
20. Sato, Y., Niceno,ˇ B., *Comput. Phys.*, 249 (2013)127–161
21. Nichita, B.A., *EPFL, Switzerland Ph.D. thesis.,* (2010)
22. Ganapathy, H., Shooshtari, A., Choo, K., Dessiatoun, S., Alshehhi, M., Ohadi, M., *Int. J. Heat Mass Transfer 65*, (2013), 62–72.
23. Sun, D.-L., Xu, J.-L., Wang, L., *Int. Commun. Heat Mass Transfer 39*(2012)1101–1106.
24. Badillo, A., *Phys. Rev. E 86*(2012)041603.
25. Badillo, A*., International Mechanical Engineering Congress and Exposition. San Diego, USA., (2013), IMECE-2013-65925.*
26. ANSYS FLUENT, Theory Guide. *Multiphase Flows,ANSYS Inc.,*November 2013, pp. 465–600 (Chapter 17)
27. Abdullahi B., *Thesis submitted to University of Birmingham*, 2015.
28. Fadhl, B., Luiz C.W., Jouhara, H.*,Appl. Therm. Eng.* 60 (1–2) (2013) 122–131.
29. Alizadehdakhel A.,Rahimi, M.,Alsairafi, A.A.,*Int. Commun. Heat Mass Transfer* 37 (3) (2010) 312–318
30. El Mghari H., Louhlia H*., Int. Commun. Heat Mass Transfer* 71 (2016)197-207.
31. Amghark.,Louhibi M.A., Salhi N., Salhi M*., J. Mater. Environ. Sci.* 8 (4) (2017) 1417
32. Rahmani k., Al-Kassir A., Benalia M., Djedid M., Ad C., Elmsellem H., Steli H., Kadmi y.,*J. Mater. Environ. Sci.* 8 (2) (2017) 566
33. El Amraoui R., El Mghari H., Obounou M., Kaddiri M., Mouqallid M., Affad E., Ait Msaad A., Garreton D., *J. Mater. Environ. Sci.* 8 (3) (2017) 1103

(2018) ; http://www.jmaterenvironsci.com